Article

Discovery Medicine 2025; 37(202): 2660–2672
https://doi.org/10.24976/Discov.Med.202537202.223

Diagnostic Value of Hand-Drawn Navigation-Guided Transbronchial Precision Bronchoalveolar Lavage Combined With mNGS in Community-Acquired Pneumonia

Sida Chen[1], Shan Xiao[1], Na Li[1], Chunxing Ye[1], Yuting Lai[1], Ling Wen[1], Yan Shen[1,*]

[1]Respiratory Department, Longgang Central Hospital, 518116 Shenzhen, Guangdong, China
*Correspondence: shenyan5902@126.com (Yan Shen)
Submitted: 11 August 2025 Revised: 3 October 2025 Accepted: 22 October 2025 Published: 20 November 2025

Background: Accurate etiological diagnosis of community-acquired pneumonia (CAP) is essential for guiding targeted therapy. However, conventional bronchoalveolar lavage (cBAL) is susceptible to contamination by commensal or background microorganisms, potentially compromising diagnostic accuracy. This study aimed to evaluate the clinical value of hand-drawn navigation-guided transbronchial precision bronchoalveolar lavage (TB-PBAL) combined with metagenomic next-generation sequencing (mNGS) in enhancing the etiological diagnosis of CAP.

Methods: A total of 50 CAP patients were enrolled in the study. Each patient underwent TB-PBAL under hand-drawn navigation guidance and cBAL. The lavage fluids obtained by these two techniques were designated as the experimental group (TB-PBAL) and the control group (cBAL), respectively. All samples were analyzed using mNGS, and detection rates of pathogens, pathogenic bacteria, and background bacteria were compared. Differences in pathogen detection rate, relative abundance of pathogenic bacteria, background bacterial detection rate, mixed infection rate, pathogenic bacteria signal-to-noise ratio (S/N ratio), and clinician preference for test reports were statistically analyzed.

Results: The overall pathogen detection rates showed no significant difference between the two groups (95.70% vs. 93.20%, $p > 0.05$). Notably, TB-PBAL demonstrated a significantly higher relative abundance of pathogenic bacteria compared with cBAL (67.42% $\pm$ 11.28% vs. 31.25% $\pm$ 9.46%, $p < 0.001$), with predominant pathogens including *Haemophilus influenzae*, *Pseudomonas aeruginosa*, and *Mycobacterium tuberculosis*. TB-PBAL yielded significantly lower background microbial interference, as evidenced by reduced background bacterial detection rates (38% vs. 64%, $p = 0.009$) and sequence counts (25.30 $\pm$ 10.60 vs. 82.70 $\pm$ 15.40, $p < 0.001$). Consequently, the signal-to-noise ratio for pathogenic bacteria was markedly higher in the TB-PBAL group (6.50 $\pm$ 2.12 vs. 3.23 $\pm$ 1.45, $p < 0.001$). In blinded clinical assessments, physicians demonstrated significantly greater preference for TB-PBAL-derived mNGS reports (50% vs. 30%, $p = 0.041$).

Conclusion: Hand-drawn navigation-guided TB-PBAL combined with mNGS significantly improves etiological diagnosis of CAP by enriching the relative abundance of true pathogens, minimizing background microbial interference, enhancing the signal-to-noise ratio, and increasing clinician confidence in sequencing results.

Keywords: community-acquired pneumonia; hand-drawn navigation; transbronchial precision bronchoalveolar lavage; conventional bronchoalveolar lavage; metagenomic next-generation sequencing; etiological diagnosis

Introduction

Community-acquired pneumonia (CAP) is a prevalent infectious disease globally, associated with marked morbidity and mortality, particularly among immunocompromised individuals, elderly patients, and those with underlying comorbidities [1,2]. The etiological spectrum of CAP is diverse, comprising bacteria, viruses, fungi, and atypical pathogens, which collectively contribute to its complex and heterogeneous clinical presentations. Accurate etiological diagnosis is essential for precise treatment and optimization of antimicrobial therapy [3–5]. Although accurate pathogen identification is critical for targeted antimicrobial therapy, conventional diagnostic approaches (including sputum culture, blood culture, and polymerase chain reaction (PCR)) frequently yield suboptimal results due to sample quality limitations, stringent culture conditions, and inherent sensitivity constraints [6,7].

Bronchoalveolar lavage (BAL) has emerged as a valuable minimally invasive technique for detecting pathogens in the lower respiratory tract, enabling direct sampling of pulmonary secretions via bronchoscopy [8]. However, conventional BAL (cBAL) presents notable limitations, including contamination by upper respiratory tract flora and environmental microorganisms, which may obscure true pathogenic signals and reduce diagnostic reli-

ability [9,10]. Over the past decade, advances in bronchoscopic navigation—such as CT-guided approaches, as well as virtual, electromagnetic, and hand-drawn navigation workflows—have been employed to improve lesion targeting and sampling precision, particularly for peripheral pulmonary lesions [11–13]. Most previous investigations, however, have focused on diagnostic yield for histopathological analysis or lesion-access performance; comparatively fewer have systematically evaluated infection-focused sample quality parameters (e.g., pathogenic relative abundance, background reads, and signal-to-noise ratio) that are directly relevant to microbiological interpretability. Against this background, we evaluated a hand-drawn navigation-guided transbronchial precision BAL (TB-PBAL) workflow as a pragmatic and cost-effective sampling optimization within the existing navigation framework. This method combines anatomical mapping with targeted sampling of affected lung segments to minimize background contamination while improving pathogen recovery.

The advent of metagenomic next-generation sequencing (mNGS) has revolutionized infectious disease diagnostics through its comprehensive, unbiased detection capability for diverse pathogens and antimicrobial resistance markers [14,15]. Although mNGS often outperforms conventional methods in pathogen identification [16], its diagnostic accuracy remains strongly influenced by sample quality, with background microbial contamination and host DNA interference posing persistent challenges [16,17]. These findings underscore the need to optimize BAL sampling techniques to reduce background noise and enhance pathogen yield, thereby maximizing the clinical utility of mNGS for CAP diagnosis and management.

This study systematically investigated the impact of TB-PBAL combined with mNGS on infection-relevant sample quality metrics in CAP, with particular emphasis on: (1) pathogenic bacterial enrichment efficiency, (2) reduction of background contamination, and (3) improvement of the signal-to-noise ratio. Through comprehensive comparison with cBAL across multiple parameters, including pathogen detection rates, pathogenic bacterial abundance, and background interference levels, we aimed to establish a practical sampling strategy that enhances the interpretability of mNGS results in CAP and facilitates personalized antimicrobial therapy.

Methods

Study Design and Participants

This was a single-center, prospective, self-controlled clinical study. Patients diagnosed with community-acquired pneumonia (CAP) were prospectively enrolled from the Respiratory Department at Longgang Central Hospital between December 2023 and April 2024. All participants met the predefined inclusion and exclusion criteria. The study protocol was reviewed and approved by the Ethics Committee of Shenzhen Longgang Central Hospital (Approval No. 2023ECPJ052) and conducted in accordance with the ethical principles outlined in the Declaration of Helsinki.

Inclusion criteria: (1) Diagnosis of CAP based on the Chinese Guidelines for the Diagnosis and Treatment of Adult Community-Acquired Pneumonia (2016 Edition) [18]; (2) Chest computed tomography (CT) revealing focal lung consolidation or ground-glass opacity with a lesion diameter $\geq$3 cm; (3) Age between 18 and 75 years, with clinical indication for bronchoscopy; (4) Provision of written informed consent by the patient or their legal representative.

Exclusion criteria: (1) Active pulmonary tuberculosis or confirmed lung malignancy; (2) Immunosuppressive conditions, including human immunodeficiency virus (HIV) infection or long-term immunosuppressive therapy; (3) Use of broad-spectrum antibiotics within the preceding 72 hours; (4) Contraindications to bronchoscopy.

Study Methods

All patients underwent electronic bronchoscopy under local anesthesia using an bronchoscope (BF-1TQ290, Olympus, Tokyo, Japan). Patients were positioned supine, and the bronchoscope was inserted through the nasal or oral route. An initial bronchoscopic examination was performed to evaluate airway anatomy and mucosal conditions. Each patient subsequently underwent two sequential bronchoalveolar lavage (BAL) procedures during the same session:

(1) Transbronchial precision BAL guided by hand-drawn navigation (TB-PBAL);

(2) Conventional BAL (cBAL).

To minimize the potential influence of procedural order on lavage fluid quality and pathogen detection, a randomized crossover design was employed. Among the 50 enrolled patients, 25 underwent cBAL followed by TB-PBAL, while the remaining 25 underwent TB-PBAL followed by cBAL. Both BAL procedures were performed in the same affected lung lobe. In all cases, a 20-MHz radial ultrasound probe (UM-S20-17S, Olympus, Tokyo, Japan) was used to confirm lesion localization before lavage, ensuring comparable sampling precision between the two techniques.

Hand-Drawn Navigation-Guided TB-PBAL

A hand-drawn, segment-level navigation workflow was employed as a low-cost, accessible optimization to target the affected subsegment while maintaining all other bronchoscopy and mNGS procedures unchanged. The hand-drawn navigation-guided TB-PBAL was performed according to a previously described protocol [11]. Before the procedure, a high-resolution computed tomography (HRCT) scan (Siemens SOMATOM Force, Siemens

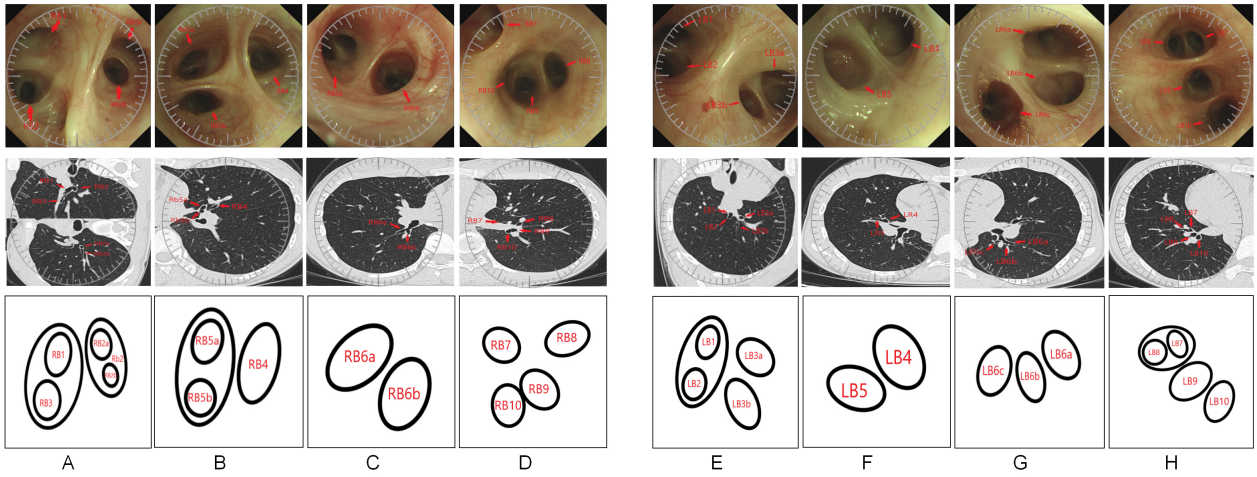

Fig. 1. Bronchoscopic views, computed tomography (CT) images, and schematic navigation maps of the patient's lungs. Panels (A–D) represent the right lung (RB: right bronchus), with Panel (A) showing the right upper lobe, Panel (B) the right middle lobe, Panel (C) the dorsal segment of the right lower lobe, and Panel (D) the basal segment of the right lower lobe. Panels (E–H) illustrate the left lung (LB: left bronchus), where Panel (E) shows the left upper lobe, Panel (F) the lingula, Panel (G) the dorsal segment of the left lower lobe, and Panel (H) the basal segment of the left lower lobe. Bottom-row ovals depict the clock-face navigation maps; red labels denote the corresponding segmental/subsegmental bronchi.

Healthineers, Erlangen, Bavaria, Germany) was performed (parameters: 120 kV tube voltage, 1 mm slice thickness, 512 × 512 matrix), and raw data were reconstructed using the Syngo Via VB10 3D imaging system (Siemens Healthineers, Erlangen, Bavaria, Germany). To ensure alignment between HRCT images and bronchoscopic visualization, image rotation was performed based on lesion location: right upper lobe lesions were rotated counterclockwise by 90°, left upper lobe lesions were rotated clockwise by 90°, and lesions located in the lower lobes, right middle lobe, or left lingular segment underwent mirror-image transformation. Lesions in the dorsal segment of the lower lobes required no rotation.

On the rotated images, bronchial openings were annotated using a clock-face notation, and a hierarchical navigation map was manually drawn. The primary bronchial opening was represented as a large circle, with successive branches denoted by smaller circles labeled with corresponding clock-face numbers, ultimately guiding the operator to the target pulmonary lesion (Fig. 1).

Real-time navigation was performed under direct bronchoscopic visualization guided by the hand-drawn map. Upon reaching the target lesion, a 20-MHz radial ultrasound probe was introduced to confirm lesion location. Subsequently, a disposable bronchoalveolar lavage catheter (LeoMed, China; Model L311890A; outer diameter 1.8 mm, working length 900 mm, single-lumen, sterile) was inserted through the working channel of the bronchoscope for precision sampling (Fig. 2). Unlike conventional cBAL, the ultra-thin and flexible design of this catheter allowed access to deeper bronchial branches (up to the 15th generation) beyond the reach of the bronchoscope tip, facilitating targeted lavage close to the actual lesion site.

The catheter featured a soft, atraumatic tip to minimize airway mucosal injury, multiple side openings to enhance aspiration and reduce mucosal suction trauma, and distal/proximal position markers for accurate localization. The transparent PEBAX tubing allowed real-time visualization of lavage fluid return. Collectively, these design elements ensured precise delivery and recovery of lavage fluid under controlled suction pressure (14–18 kPa; 105–140 mmHg), enhancing sample quality and minimizing contamination.

Sterile normal saline (37 °C) was instilled using a micro-fractional perfusion approach, and at least 30 mL of lavage fluid was retrieved under negative pressure. The recovered sample was designated as the experimental group (TB-PBAL).

Conventional Bronchoalveolar Lavage (cBAL)

Conventional bronchoalveolar lavage (cBAL) was performed in the same lesion-bearing lung lobe as TB-PBAL. In this approach, the bronchoscope was advanced into a segmental bronchus guided by anatomical landmarks rather than navigation mapping. To verify lesion localization, a 20-MHz radial ultrasound probe was utilized, consistent with the TB-PBAL protocol. After confirming the target site, a disposable double-lumen lavage catheter (Leomed, China; Model L312409B; outer diameter 2.4 mm, working length 900 mm) was introduced through the bronchoscope.

Due to its larger diameter (3–5 mm range), this catheter could only reach approximately the 6th generation

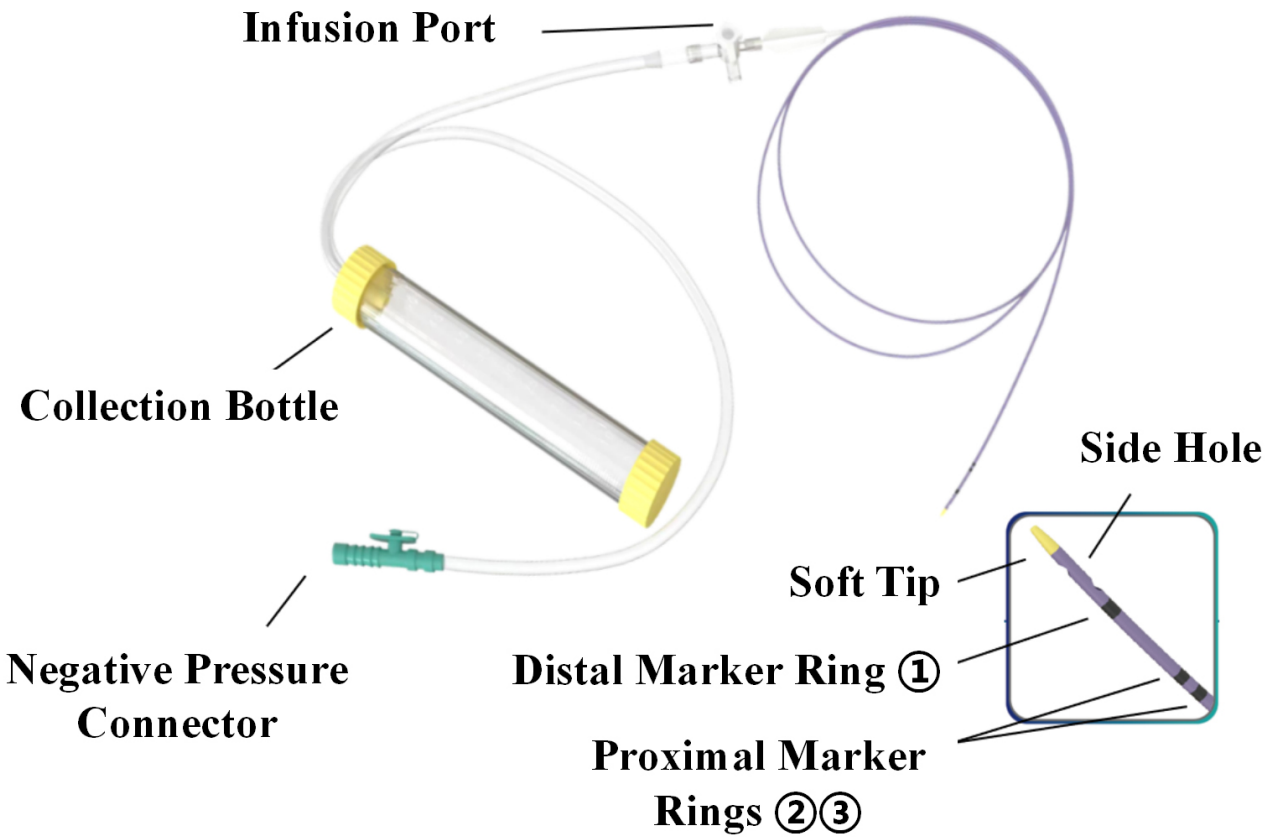

Fig. 2. Structural schematic of the disposable bronchoalveolar lavage catheter.

bronchi, thus limiting distal sampling compared with TB-PBAL, which could extend to the 15th generation bronchi. Subsequently, 60 mL of sterile saline pre-warmed to 37 °C was instilled in three separate 20 mL aliquots and aspirated under negative pressure. A minimum recovery volume of 30 mL was required for downstream analyses. The lavage fluid obtained using this procedure was designated as the control group (cBAL).

Sample Processing

All bronchoalveolar lavage fluid (BALF) specimens obtained from both procedures were immediately processed in a Class II biosafety cabinet. Using aseptic technique, samples were aliquoted into 1 mL portions in pre-sterilized, RNase/DNase-free cryogenic vials (Corning, Cat. No. 430659, USA). The processed aliquots were rapidly transferred to –80 °C ultra-low temperature freezers (Thermo Scientific Forma 900 series, USA) within 30 minutes of collection to maintain sample integrity. For subsequent transport to the sequencing facility, all samples were kept on dry ice to ensure an uninterrupted cold chain. Notably, all specimens underwent direct single-pass processing without intermediate freeze-thaw cycles before metagenomic next-generation sequencing (mNGS) analysis.

Metagenomic Next-Generation Sequencing (mNGS) Analysis

BALF samples were first centrifuged at 300 ×g for 10 minutes (Eppendorf 5810R Centrifuge, Germany) to remove cellular components, followed by a second centrifugation at 12,000 ×g for 10 minutes to collect the supernatant. Total nucleic acids were extracted using the QIAamp DNA Micro Kit (Qiagen, Cat. No. 56304, Germany) following the manufacturer's standard protocol. DNA concentration and purity were determined using a NanoDrop 2000 spectrophotometer (Thermo Fisher, USA), while DNA integrity was evaluated by 1% agarose gel electrophoresis using the Bio-Rad Mini-Sub Cell GT System (Bio-Rad Laboratories, Cat. No. 170-4486, CA, USA).

Sequencing libraries were prepared using the NEBNext Ultra DNA Library Prep Kit for Illumina (New England Biolabs, Cat. No. E7645, USA). Genomic DNA was fragmented to approximately 350 bp and subsequently amplified by PCR. Library quality and fragment size distribution were evaluated using the Agilent 2100 Bioanalyzer system (Agilent Technologies, Cat. No. 5067-4626, USA). Paired-end sequencing (150 bp) was performed on the Illumina NovaSeq 6000 platform (Illumina, USA) with a minimum sequencing depth of 20 million reads per sample.

Raw sequencing reads were subjected to stringent quality control procedures, including removal of low-quality reads, human-derived sequences, duplicate reads, and potential environmental contaminants. High-quality non-human reads were retained and taxonomically classified against the NCBI RefSeq microbial genome database (https://www.ncbi.nlm.nih.gov/refseq/) to identify potential pathogenic organisms.

Outcome Measures

Pathogen Distribution and Detection Rate

Pathogens were defined as microorganisms successfully identified by mNGS. The overall pathogen detection rate (PDR) was calculated as the proportion of samples in which at least one pathogen was detected, using the formula:

PDR = (Number of samples with $\geq$1 pathogen detected/Total number of samples tested) $\times$100%.

The specific pathogen detection rate (SPDR) represented the proportion of samples in which a particular pathogen was detected at least once, calculated as:

SPDR = (Number of samples positive for a specific pathogen/Total number of samples tested) $\times$ 100%.

Relative Abundance of Pathogenic Bacteria (RAPB)

The relative abundance of an individual pathogenic bacterium was defined as the proportion of sequencing reads assigned to that specific pathogen (e.g., *Haemophilus influenzae*) relative to the total microbial sequencing reads:

RAPB = (Number of sequencing reads for the pathogenic bacterium/Total number of microbial sequencing reads) $\times$ 100%.

The total relative abundance of pathogenic bacteria was calculated as the sum of sequencing reads assigned to all pathogenic bacteria taxa (including *H. influenzae*, *Pseudomonas aeruginosa*, *Mycobacterium tuberculosis*, etc.) relative to the total microbial sequencing reads. The Kraken2 and Bracken bioinformatics tools were used to quantify pathogenic bacterial relative abundance.

Definition of Pathogenic Bacteria

In this study, pathogenic bacteria were defined as bacterial species detected by mNGS in BALF samples that are recognized respiratory pathogens and clinically consistent with the patient's presentation, including symptoms and radiological findings. Pathogen classification was independently evaluated and verified by two experienced respiratory physicians.

Detection Rate and Sequencing Reads of Background Bacteria

In this study, background bacteria refer to taxa detected by mNGS that—based on clinical and radiological context—are unlikely to represent causative pathogens. Predefined, auditable rules were applied: (i) low-abundance colonizers common to the oral or upper airway (e.g., *Haemophilus parainfluenzae*) were classified as background when $<$1% relative abundance (RA) or $<$10 reads per million (RPM) and lacking clinical concordance [19]; (ii) taxa detected in run-matched negative controls (NTC) at or above the NTC 99th percentile (or mean + 3 SD) were designated contaminants; (iii) ultra-low reads ($<$0.01% RA or $<$3 RPM) were excluded as background noise; (iv) when run-matched NTCs were unavailable, a historical NTC baseline from the same laboratory (rolling 3-month window) was applied [20].

The overall background bacteria detection rate (BDR) was defined as the proportion of samples in which at least one background bacterium was detected:

BDR = (Number of samples with $\geq$1 background bacterium detected/Total number of samples tested) $\times$ 100%.

The specific background bacteria detection rate (SBDR) represented the proportion of samples in which a particular background bacterium was identified:

SBDR = (Number of samples with the specific background bacterium detected/Total number of samples tested) $\times$ 100%.

Signal-to-Noise Ratio (S/N Ratio) of Pathogenic Bacteria

The S/N ratio was defined as the ratio of sequencing reads corresponding to pathogenic bacteria to those assigned to background bacteria. A higher S/N ratio indicated stronger pathogenic bacterial signals with reduced background interference.

S/N = Number of pathogenic bacterial sequencing reads/Number of background bacterial sequencing reads.

Mixed Infection Detection Rate (MIDR)

MIDR was defined as the proportion of samples in which two or more potential pathogenic bacteria were co-detected.

MIDR = (Number of samples with $\geq$2 detected pathogenic bacteria/Total number of samples tested) $\times$ 100%.

Clinicians' Interpretation Preference for mNGS Reports

Clinicians' interpretation preference for mNGS reports between the experimental and control groups was evaluated. The clinicians' preference rate (CPR) was defined as the proportion of clinicians selecting mNGS reports from a specific group as the primary reference for clinical decision-making:

CPR = (Number of clinicians selecting the mNGS report from a specific group/Total number of clinicians surveyed) $\times$ 100%.

In a double-blinded evaluation, at least three experienced clinicians independently reviewed mNGS reports from both groups, and their selection preferences were recorded.

Table 1. Baseline demographic and clinical characteristics of the study population (n = 50).

Characteristic	Value
Age (years)	58.32 ± 12.47
Gender, n (%)	
Male	28 (56%)
Female	22 (44%)
Baseline respiratory rate (breaths/minute)	22.53 ± 3.21
Baseline heart rate (beats/minute)	88.62 ± 10.38
Baseline oxygen saturation (SpO_2)	93.27% ± 2.46%
Baseline blood pressure (mmHg)	128/76 ± 10/8
Oxygen flow rate (L/minute)	2.48 ± 1.02
Lavage site, n (%)	
Left upper lobe	5 (10%)
Left middle lobe	3 (6%)
Left lower lobe	12 (24%)
Right upper lobe	8 (16%)
Right middle lobe	4 (8%)
Right lower lobe	18 (36%)
Purulent airway secretions, n (%)	
Yes	22 (44%)
No	28 (56%)

Statistical Analysis

All statistical analyses were performed using SPSS 26.0 (IBM, USA). The normality of continuous variables was assessed using the Shapiro–Wilk test. Normally distributed data were presented as mean ± standard deviation (Mean ± SD), whereas non-normally distributed data were expressed as median (interquartile range, IQR). For within-group comparisons, paired *t*-tests were applied to normally distributed variables, while the Wilcoxon signed-rank test was used for non-normally distributed data. Categorical variables were expressed as frequency (percentage). Between-group comparisons of categorical variables were conducted using the chi-square test when the expected frequency per cell was ≥5; otherwise, Fisher's exact test was applied. A two-tailed p-value < 0.05 was considered statistically significant.

Results

General Clinical Characteristics of Patients

A total of 50 patients with community-acquired pneumonia (CAP) were enrolled in this study, with a mean age of 58.32 ± 12.47 years. Among them, 28 (56%) were male and 22 (44%) were female. The baseline respiratory rate was 22.53 ± 3.21 breaths per minute, and the mean heart rate was 88.62 ± 10.38 beats per minute. Baseline oxygen saturation (SpO_2) averaged 93.27% ± 2.46%, while the mean arterial blood pressure was 128/76 ± 10/8 mmHg. The mean supplemental oxygen flow rate was 2.48 ± 1.02 L/min.

In terms of the distribution of lavage sites, the right lower lobe was the most frequently sampled (18 cases, 36.0%), followed by the left lower lobe (12 cases, 24.0%). Sampling from the left upper lobe, left middle lobe, right upper lobe, and right middle lobe accounted for 10%, 6%, 16%, and 8% of cases, respectively. Purulent secretions were observed within the airways in 22 patients (44%), while 28 patients (56%) showed no visible purulence (Table 1).

Comparison of Parameters Between TB-PBAL and Conventional BAL

When comparing the two lavage techniques, the experimental group (TB-PBAL) demonstrated statistically significant advantages over the control group (cBAL) across multiple intraoperative parameters (Table 2). Notably, the median number of coughs recorded in the TB-PBAL group was 2 (IQR: 1–3), significantly lower than the 4 (IQR: 3–6) observed in the cBAL group ($z = –4.858$, $p < 0.001$).

Furthermore, the maximum respiratory rate and peak heart rate in the TB-PBAL group were 24.33 ± 2.81 breaths per minute and 92.52 ± 8.74 beats per minute, respectively, both significantly lower than those in the cBAL group (28.64 ± 3.53 breaths per minute, 98.23 ± 10.15 beats per minute; $t = 5.236$, $p < 0.001$; $t = 3.122$, $p = 0.003$, respectively). The lowest oxygen saturation during the procedure was 90.51% ± 3.22% in the TB-PBAL group, significantly higher than 85.34% ± 4.13% in the cBAL group ($t = 5.893$, $p < 0.001$).

Although the overall incidence of bleeding did not differ significantly between groups (6% vs. 16%; $\chi^2 = 1.634$, $p = 0.201$), the rate of mucosal bleeding was markedly lower in the TB-PBAL group (10% vs. 26%; $\chi^2 = 4.336$, $p = 0.037$).

Table 2. Comparison of relevant indicators during catheter lavage and conventional lavage.

Indicator	Experimental group (n = 50)	Control group (n = 50)	$z/\chi^2/t$	*p*-value
Cough frequency (times)	2 (1–3)	4 (3–6)	–4.858	<0.001
Highest respiratory rate (breaths/minute)	24.33 ± 2.81	28.64 ± 3.53	5.236	<0.001
Highest heart rate (beats/minute)	92.52 ± 8.74	98.23 ± 10.15	3.122	0.003
Lowest oxygen saturation (SpO_2, %)	90.51 ± 3.22	85.34 ± 4.13	5.893	<0.001
Bleeding, n (%)	3 (6%)	8 (16%)	1.634	0.201
Mucosal bleeding, n (%)	5 (10%)	13 (26%)	4.336	0.037
Lavage volume (mL)	60 ± 0	60 ± 0	0	1
Recovered volume (mL)	42.52 ± 4.24	33.76 ± 5.49	8.293	<0.001
Procedure duration (minute)	15.73 ± 3.45	10.55 ± 2.78	8.469	<0.001
Other complications, n (%)	1 (2%)	3 (6%)	0	1

Table 3. Distribution of pathogen categories and detection rates in BALF samples between the two groups.

Category	Experimental group (n = 50)	Control group (n = 50)	χ^2	*p*-value
Bacteria (≥1 species)	37 (74%)	32 (64%)	1.169	0.280
Mycobacteria	9 (18%)	7 (14%)	0.298	0.585
Viruses (≥1 species)	18 (36%)	15 (30%)	0.407	0.523
Fungi	4 (8%)	4 (8%)	0	1
Atypical pathogens	5 (10%)	4 (8%)	0	1
Other pathogens	4 (8%)	2 (4%)	0.177	0.674
Overall pathogen detection rate (PDR)	48 (95.70%)	47 (93.20%)	0	1

Note: Since some patients were positive for more than one pathogen, the sum of individual percentages may exceed the total percentage of unique infections. Data for "Bacteria" and "Mycobacteria" were deduplicated.

Both groups received an identical lavage volume of 60 mL. However, the recovered fluid volume was significantly greater in the TB-PBAL group (42.52 ± 4.24 mL) compared with the cBAL group (33.76 ± 5.49 mL; $t = 8.293$, $p < 0.001$), indicating superior sampling efficiency. The procedure duration was also longer in the TB-PBAL group than in the cBAL group (15.73 ± 3.45 minutes vs. 10.55 ± 2.78 minutes; $t = 8.469$, $p < 0.001$), likely due to the finer instruments and the requirement for precise lesion targeting. The incidence of other intraoperative complications remained low and showed no significant difference between groups (2% vs. 6%; $\chi^2 = 0$, $p > 0.05$).

Pathogen Classification and Detection Rate Distribution

Metagenomic next-generation sequencing (mNGS) identified 31 distinct pathogens across the two groups. The overall pathogen detection rates were comparable between the TB-PBAL group (95.70%) and the cBAL (93.20%) ($p > 0.05$) (Fig. 3; Table 3). Bacterial pathogens were detected in 74% of TB-PBAL samples and 64% of cBAL samples ($p > 0.05$). Although the proportion was numerically higher in TB-PBAL, the difference was not statistically significant.

No significant differences were observed for common bacterial species, including *Streptococcus pneumoniae, Haemophilus influenzae, Staphylococcus aureus, Legionella pneumophila*, and *Bordetella pertussis* ($p > 0.05$). The detection rate of *Pseudomonas aeruginosa* was higher in the TB-PBAL group (14% vs. 6%), but the difference did not reach statistical significance ($p > 0.05$). *Mycobacterium* species were identified in 18% of the TB-PBAL group and 14% of the cBAL group ($p > 0.05$), with no significant group differences across specific species.

Viral detection rates were 36% in the TB-PBAL group and 30% in the cBAL group ($p > 0.05$), with no significant variation among individual viral species. Similarly, fungal (8.0% vs. 8%), atypical (10% vs. 8%), and other pathogens (8% vs. 4%) showed no statistically significant differences ($p > 0.05$). Overall, the diagnostic yields of mNGS were comparable between the two techniques.

Comparison of the Relative Abundance of Pathogenic Bacteria in BALF Samples

This study compared the relative abundance of major pathogenic bacteria between the two groups (Table 4). The relative abundance of *Streptococcus pneumoniae* in the experimental group was 12.15% ± 3.02%, slightly higher than the 10.08% ± 2.47% observed in the control group ($t = 2.123$, $p = 0.037$). *Haemophilus influenzae* showed a significantly higher abundance in the experimental group compared with the control group ($t = 8.452$, $p < 0.001$), indicating improved pathogen enrichment. Similarly, the relative abundance of *Mycobacterium tuberculosis* was higher in the experimental group than in the control group ($t = 6.482$, $p < 0.001$). A comparable trend was also observed for *Pseudomonas aeruginosa* ($t = 5.003$, $p < 0.001$).

No statistically significant differences in relative abundance were detected for other pathogens, including

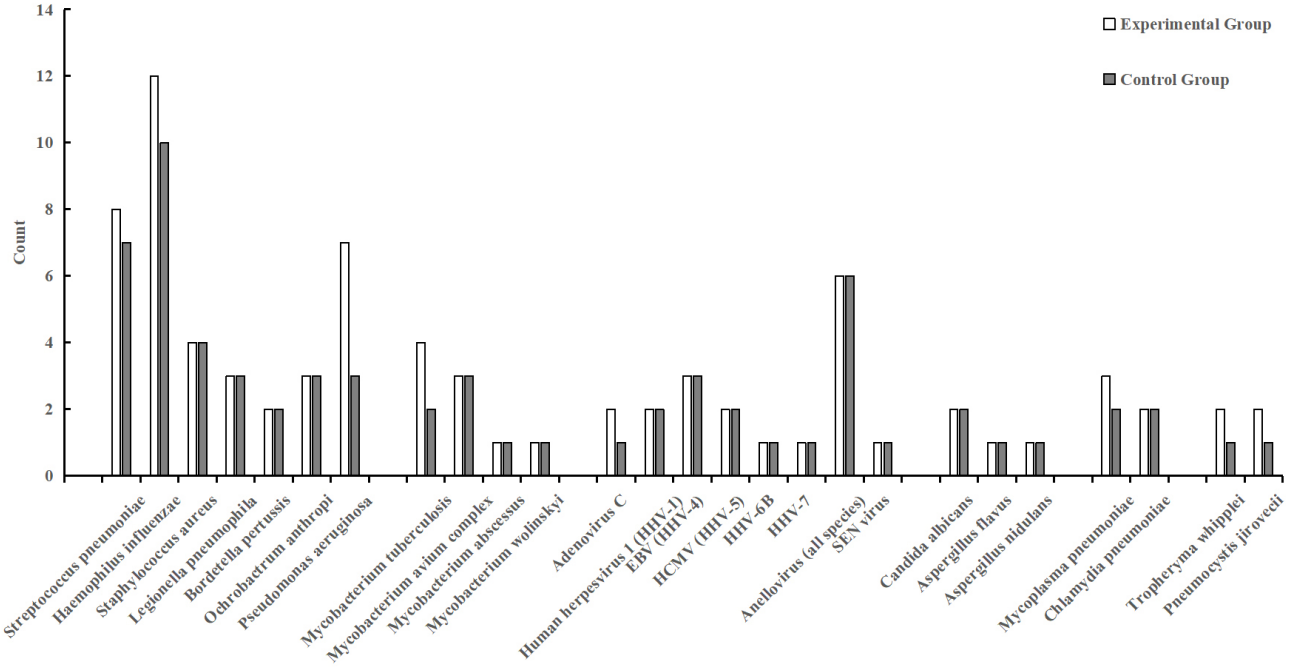

Fig. 3. Detection results of pathogenic bacteria in alveolar lavage fluid between the two groups.

Table 4. Comparison of the relative abundance of pathogenic bacteria in BALF samples between the two groups.

Category/pathogen	Experimental group (n = 50)	Control group (n = 50)	*t*/z	*p*-value
Bacteria				
Streptococcus pneumoniae	12.15 ± 3.02	10.08 ± 2.47	*t* = 2.123	0.037
Haemophilus influenzae	22.36 ± 4.12	10.27 ± 3.05	*t* = 8.452	<0.001
Staphylococcus aureus	5.00 (4.00–6.00)	5.00 (4.00–6.00)	z = 0.214	0.831
Legionella pneumophila	3.05 (2.00–4.00)	2.48 (2.00–3.00)	z = 1.153	0.249
Bordetella pertussis	2.10 (1.00–2.00)	2.05 (1.00–2.00)	z = 0.185	0.854
Mycobacteria				
Mycobacterium tuberculosis	8.12 ± 3.14	3.06 ± 1.52	*t* = 6.482	<0.001
Mycobacterium avium complex	4.02 (3.00–5.00)	4.08 (3.00–5.00)	z = 0.142	0.887
Mycobacterium abscessus	1.00 (1.00–1.00)	1.00 (1.00–1.00)	z= 0.071	0.944
Other bacteria				
Pseudomonas aeruginosa	10.24 ± 3.15	4.12 ± 1.48	*t* = 5.003	<0.001
Viruses				
Human adenovirus C	3.02 (2.00–4.00)	2.56 (2.00–3.00)	z = 1.583	0.114
Human herpesvirus 1 (HHV-1)	2.00 (2.00–2.00)	2.00 (2.00–2.00)	z = 0.132	0.895
Fungi				
Aspergillus flavus	2.00 (2.00–2.00)	2.00 (2.00–2.00)	z = 0.095	0.924
Atypical pathogens				
Mycoplasma pneumoniae	3.08 (2.00–3.00)	3.04 (2.00–3.00)	z = 0.076	0.939
Chlamydia pneumoniae	2.02 (2.00–2.00)	2.00 (2.00–2.00)	z = 0.118	0.906
Overall relative abundance of pathogenic bacteria	67.42 ± 11.28	31.25 ± 9.46	*t* = 8.001	<0.001

Note: Data are expressed as relative abundance (%).

Staphylococcus aureus, *Legionella pneumophila*, *Bordetella pertussis*, *Mycobacterium avium* complex, *Mycobacterium abscessus*, as well as viral and fungal species ($p > 0.05$). Notably, the total relative abundance of all detected pathogenic bacteria was significantly higher in the experimental group than in the control group ($t = 8.001$, $p < 0.001$), suggesting that TB-PBAL provided enhanced pathogen enrichment compared with conventional BAL.

Table 5. Comparison of background microorganism detection rates and sequence counts in BALF samples between the two groups.

Background microorganism	Detection rate, n (%)		χ^2	*p*-value	Sequence count [Mean ± SD/Median (IQR)]		z/*t*	*p*-value
	Experimental group (n = 50)	Control group (n = 50)			Experimental group (n = 50)	Control group (n = 50)		
Bacteria								
Tropheryma whipplei	4 (8%)	8 (16%)	0.852	0.356	20 (15–26)	50 (42–58)	z = –1.421	0.161
Ochrobactrum anthropi	6 (12%)	12 (24%)	2.439	0.118	22.00 ± 7.00	55.00 ± 12.00	*t* = –3.853	<0.001
Mycobacterium wolinskyi	2 (4%)	5 (10%)	0.614	0.433	18 (14–22)	45 (38–52)	z = –1.602	0.115
Viruses								
SEN virus	5 (10%)	10 (20%)	1.961	0.161	15 (12–18)	40 (34–46)	z = –1.572	0.121
Circovirus	6 (12%)	12 (24%)	2.439	0.118	18 (14–22)	50 (42–58)	z = –1.463	0.148
Circovirus type 5	3 (6%)	6 (12%)	0.488	0.485	12 (10–14)	30 (25–35)	z = –1.554	0.125
Circovirus type 15	3 (6%)	6 (12%)	0.488	0.485	10 (8–12)	28 (24–32)	z = –1.591	0.116
Circovirus type 24	2 (4%)	4 (8%)	0.177	0.674	8 (7–9)	20 (18–22)	z = –1.562	0.123
Circovirus type 29	2 (4%)	4 (8%)	0.177	0.674	7 (6–8)	18 (16–20)	z = –1.482	0.142
Epstein–Barr virus	4 (8%)	9 (18%)	1.415	0.234	16.00 ± 6.00	42.00 ± 8.00	*t* = –1.623	0.108
Human cytomegalovirus	4 (8%)	8 (16%)	0.852	0.356	14.00 ± 5.00	38.00 ± 7.00	*t* = –1.556	0.124
Human herpesvirus 6B	2 (4%)	5 (10%)	0.614	0.433	10 (9–11)	30 (28–32)	z = –1.537	0.13
Human herpesvirus 7	2 (4%)	5 (10%)	0.614	0.433	9 (8–10)	28 (26–30)	z = –1.325	0.194
Fungi								
Pneumocystis jirovecii	3 (6%)	8 (16%)	1.634	0.201	12 (10–14)	35 (30–40)	z = –1.494	0.138
Aspergillus nidulans	2 (4%)	5 (10%)	0.614	0.433	10 (9–11)	28 (26–30)	z = –1.423	0.158
Total background microorganisms	19 (38%)	32 (64%)	6.763	0.009	25.30 ± 10.60	82.70 ± 15.40	*t* = –4.824	<0.001

Note: IQR, interquartile range.

Table 6. Comparison of mixed infection rate, pathogenic bacteria signal-to-noise ratio (S/N), and NGS report selection rate between the two groups.

Group	Mixed infection rate, n (%)	S/N ratio (mean ± SD)	NGS report selection rate, n (%)
Experimental group (n = 50)	6 (12.5%)	6.50 ± 2.12	25 (50.0%)
Control group (n = 50)	6 (12.5%)	3.23 ± 1.45	15 (30.0%)
χ^2/t	0	9.002	4.167
p-value	1	<0.001	0.041

Comparison of Background Bacteria Detection Rates and Sequencing Read Counts in BALF Samples

As shown in Table 5, both the detection rates and sequencing read counts of background microorganisms were generally lower in the TB-PBAL group compared with the cBAL group. Most individual bacterial, viral, and fungal taxa exhibited no statistically significant differences between groups ($p > 0.05$). However, *Ochrobactrum anthropi* represented an exception, showing a lower detection rate in the TB-PBAL group compared with the cBAL group (12% vs. 24%; $\chi^2 = 2.439$, $p > 0.05$), with significantly reduced sequencing read count (22.00 ± 7.00 vs. 55.00 ± 12.00; $t = –3.853$, $p < 0.001$).

Importantly, when background microorganisms were analyzed collectively, the TB-PBAL group demonstrated a significantly lower overall detection rate (38% vs. 64%; $p = 0.009$) and markedly reduced sequencing read counts (25.30 ± 10.60 vs. 82.70 ± 15.40; $t = –4.824$, $p < 0.001$). These findings indicate that TB-PBAL effectively suppresses background microbial interference, thereby enhancing the specificity of pathogen detection compared with conventional BAL.

Comparison of Mixed Infection Rate, Signal-to-Noise Ratio, and NGS Report Selection Rate in BALF Samples

Table 6 summarizes the mixed infection rate, signal-to-noise (S/N) ratio of pathogenic bacteria, and NGS report selection rate. Both groups demonstrated a mixed infection rate of 12.5%, with no statistically significant difference ($p > 0.05$). However, the S/N ratio in the experimental group was significantly higher than in the control group (6.50 ± 2.12 vs. 3.23 ± 1.45; $t = 9.002$, $p < 0.001$), indicating a more robust and stable pathogenic signal in the TB-PBAL samples. Additionally, the NGS report selection rate was 50% in the experimental group compared with 30% in the control group ($\chi^2 = 4.167$, $p = 0.041$), reflecting greater clinical acceptance and diagnostic reliability of TB-PBAL test results.

Discussion

This study aimed to address the limitations of BAL in the etiological diagnosis of CAP, particularly the dilution of true pathogenic signals by background microbial contamination. We evaluated the clinical utility of hand-drawn navigation-guided TB-PBAL combined with mNGS. Accurate pathogen identification is essential for guiding targeted antimicrobial therapy and optimizing anti-infective treatment strategies in CAP. However, conventional diagnostic approaches often fall short due to inadequate pathogen enrichment and poor differentiation from background flora [6,7]. Within this context, our findings demonstrate that TB-PBAL significantly increases the relative abundance of pathogenic bacteria, reduces background microbial interference, and enhances the signal quality of mNGS output. Collectively, these improvements contribute to greater diagnostic accuracy and clinical interpretability.

The enrichment of pathogenic bacteria is a key determinant of mNGS diagnostic efficacy, as a higher relative abundance reflects a stronger pathogen signal, thereby enhancing clinicians' confidence in interpretation and treatment decisions [21]. In this study, the TB-PBAL group demonstrated significantly higher relative abundances of *Haemophilus influenzae* (22% vs. 10%) and *Mycobacterium tuberculosis* (8% vs. 3%) compared with the cBAL group. Notably, *Pseudomonas aeruginosa* accounted for 10.0% of microbial reads in the TB-PBAL group—representing a 150% increase over the control. These findings align with a previous study employing precision sampling techniques, such as electromagnetic navigational bronchoscopy (ENB), for pathogen detection in pulmonary infections [22]. Previous studies have emphasized that bronchoscopic navigation not only minimizes sampling deviations but also enhances diagnostic yield by enabling the acquisition of higher-quality specimens for mNGS analysis [23,24]. Taken together, these findings reinforce the clinical utility of TB-PBAL in enhancing pathogen enrichment and improving the analytical reliability of mNGS in CAP diagnostics.

Reducing background bacterial interference represents another critical factor for improving the specificity of mNGS. Background contamination—originating from host DNA, upper respiratory tract commensals, or laboratory-derived artefacts—can obscure true pathogen signals and reduce diagnostic accuracy [25,26]. In our study, TB-PBAL significantly reduced the sequencing read counts of background organisms such as *Haemophilus parainfluenzae* by 60%–75% and decreased the overall background bacterial detection rate by 38.7%. This improvement is likely due to: (1) the use of a dedicated lavage catheter, which minimizes contamination from the supraglottic re-

gion and limits the introduction of nonpathogenic flora; (2) precise lesion localization through hand-drawn navigation, which avoids sampling from unaffected lung segments and reduces interference from commensals; and (3) an optimized lavage protocol that suppresses the cough reflex, improving stability and reproducibility of sampling [27]. These findings are consistent with those reported by Nan *et al*. [16], who demonstrated that optimized sampling techniques could markedly enhance mNGS performance, ultimately supporting more accurate and individualized clinical decision-making.

Enhancement of the signal-to-noise (S/N) ratio is critical for stabilizing mNGS detection. In our study, TB-PBAL achieved an S/N ratio of 6.5, representing an approximate 103% improvement over conventional BAL. This enhancement likely results from two key factors: first, TB-PBAL enriches the bronchoalveolar lavage fluid with neutrophils, which contain 3–5 times higher bacterial loads than bronchial secretions, thereby increasing the concentration of pathogen DNA [28,29]; second, given that the mNGS detection limit (LoD) is inversely related to pathogen concentration, the increased abundance of pathogenic bacteria in TB-PBAL samples led to a 42.9% higher number of species exceeding the conventional LoD threshold (5%) compared with the control (9 vs. 6 species). These findings underscore the significance of optimizing sampling strategies to improve pathogen detection accuracy, as supported by previous studies [11–13].

Moreover, TB-PBAL appears to enhance clinical decision-making confidence. In a double-blind evaluation, mNGS reports derived from TB-PBAL samples were preferred by clinicians in 50% of cases, compared to only 30% for conventional samples ($p < 0.05$). This suggests that the higher pathogen signal provided by TB-PBAL confers greater clinical credibility and utility, consistent with previous research demonstrating a strong correlation between enhanced pathogen signals and increased clinician trust in mNGS results [30]. Collectively, these outcomes highlight the diagnostic advantages of TB-PBAL in improving pathogen detection accuracy, facilitating clearer result interpretation, and supporting more precise, individualized anti-infective treatment strategies.

While TB-PBAL demonstrated multiple technical advantages over conventional BAL, its diagnostic efficacy remains highly dependent on accurate lesion localization. The precision sampling capability of the lavage catheter must be supported by reliable navigational guidance, such as the hand-drawn navigation technique employed in this study. Without accurate mapping of the lesion site, the catheter may be inadvertently directed to unaffected bronchial segments, resulting in non-representative samples. In such cases, TB-PBAL could paradoxically yield poorer results than conventional BAL. Unlike TB-PBAL, conventional lavage typically samples multiple pulmonary segments, thereby increasing the likelihood of capturing pathogens even without precise localization. This highlights a critical trade-off between targeted accuracy and sampling breadth. Therefore, the clinical application of TB-PBAL depends not only on operator expertise but also on high-quality imaging and precise localization. The hand-drawn navigation method used in this study effectively improves lesion targeting and sampling precision.

Hand-drawn navigation is not intended to replace CT-, VBN-, ENB-, or robotic-navigation platforms that provide superior localization accuracy and instrument stability. Instead, it serves as a pragmatic and cost-effective complementary approach for well-defined segmental or subsegmental infectious lesions, particularly in resource-constrained settings. Consistent with this positioning, our study evaluated infection-focused sample quality metrics, such as pathogenic relative abundance, background reads, and S/N ratio, rather than histopathologic or biopsy yield.

Nevertheless, several limitations should be acknowledged. First, the single-center design may introduce selection bias, and multicenter studies are warranted to validate the generalizability of these findings. Second, quantitative assessments of navigation accuracy (e.g., measurements of localization error in millimeters) were not performed. Additionally, the absence of a significant difference in mixed infection rates may be related to the relatively small sample size, increasing the likelihood of a type II error. This self-controlled design minimized confounding from fixed patient factors (e.g., secretion purulence), as each patient served as his or her own control. However, our study was not powered to detect the effects of the interaction between technique and purulence. Thus, larger, multicenter cohorts are needed to evaluate potential effect modification. Future research could integrate artificial intelligence-assisted navigation systems to further refine sampling path planning and incorporate cost-effectiveness analyses to evaluate the health-economic implications of TB-PBAL.

Conclusion

This study demonstrates that hand-drawn navigation-guided transbronchial precision bronchoalveolar lavage (TB-PBAL) combined with mNGS significantly enhances the accuracy of etiological diagnosis in CAP. The principal advantages of this technique include increased relative abundance of pathogenic bacteria, reduced background microbial contamination, improved signal stability, and enhanced clinical interpretability, thereby supporting optimized clinical decision-making. Future investigations should aim to refine procedural protocols, standardize application parameters, and expand clinical validation to facilitate broader implementation of this technique in precision pulmonary infection diagnostics.

Availability of Data and Materials

All data generated or analyzed during this study are included in this published article. Further enquiries can be directed to the corresponding author.

Author Contributions

SC and SX were guarantors of the integrity of the entire study and made substantial contributions to study conception and design, clinical investigation, data analysis, statistical analysis, and drafting of the manuscript. NL contributed to literature review, patient recruitment and data acquisition, assisted with data analysis and interpretation, and participated in drafting and critical revision of the manuscript for important intellectual content. CY and YL performed experimental studies and data curation, contributed to data analysis/interpretation and figure/table preparation, and participated in drafting and critical revision of the manuscript. LW contributed to literature review, data acquisition, visualization, and participated in drafting and critical revision of the manuscript. YS contributed to study conception and design, supervision, data analysis and interpretation, and critical revision of the manuscript for important intellectual content. All authors have been involved in drafting the manuscript or revising it critically for important intellectual content, have given final approval of the version to be published, and agreed to be accountable for all aspects of the work in ensuring that questions related to the accuracy or integrity of any part of the work are appropriately investigated and resolved.

Ethics Approval and Consent to Participate

The study protocol was reviewed and approved by the Medical Ethics Committee (Institutional Review Board) of Shenzhen Longgang Central Hospital, China (Approval No. 2023ECPJ052; 24 August 2023). All procedures complied with the Declaration of Helsinki and applicable regulations. Written informed consent was obtained from all participants.

Acknowledgment

Not applicable.

Funding

This work was supported by the Longgang District Medical and Health Technology Research Project (Grant number LGKCYLWS2023014) and the Longgang Medical Discipline Construction Fund.

Conflict of Interest

The authors declare no conflict of interest.

References

[1] Vaughn MV, Dickson RP, Horowitz JK, Flanders SA. Community-Acquired Pneumonia: A Review. JAMA. 2024; 332: 1282–1295. https://doi.org/10.1001/jama.2024.14796.

[2] Yılmaz E, Benli A, Başaran S, Şimşek-Yavuz S, Cagatay A, Oncul MO, *et al*. Community-Acquired Pneumonia in the Immunocompromised Patients: An Observational Study from a Single Center, TURKEY. Infection and Drug Resistance. 2024; 17: 4875–4885. https://doi.org/10.2147/IDR.S480520.

[3] Arnold FW, Summersgill JT, Ramirez JA. Role of Atypical Pathogens in the Etiology of Community-Acquired Pneumonia. Seminars in Respiratory and Critical Care Medicine. 2016; 37: 819–828. https://doi.org/10.1055/s-0036-1592121.

[4] Nambafu J, Achakolong M, Mwendwa F, Bwika J, Riunga F, Gitau S, *et al*. A prospective observational study of community acquired pneumonia in Kenya: the role of viral pathogens. BMC Infectious Diseases. 2021; 21: 703. https://doi.org/10.1186/s12879-021-06388-x.

[5] Chean D, Windsor C, Lafarge A, Dupont T, Nakaa S, Whiting L, *et al*. Severe Community-Acquired Pneumonia in Immunocompromised Patients. Seminars in Respiratory and Critical Care Medicine. 2024; 45: 255–265. https://doi.org/10.1055/s-0043-1778137.

[6] Joelsons D, Alencar CS, Pinho JRR, Ho YL. Investigation of etiology of community-acquired pneumonia in hospitalized patients in a tertiary hospital of São Paulo City, Brazil. The Brazilian Journal of Infectious Diseases: an Official Publication of the Brazilian Society of Infectious Diseases. 2023; 27: 103690. https://doi.org/10.1016/j.bjid.2023.103690.

[7] Ho EC, Asturias EJ, Butler M, Simmons D, Dominguez SR. P-2221. Clinical utility and sensitivity of plasma metagenomic microbial cell-free DNA sequencing in children with complicated pneumonia. Open Forum Infectious Diseases. 2025; 12(Supplement_1): ofae631-ofae2375.

[8] Patrucco F, Bellan M, Martinotti D, Ielo G, Iovine PR, Mascheroni M, *et al*. The Role of Bronchoalveolar Lavage in Therapeutic Antimicrobial Choices for Hematologic Patients with Pulmonary Infiltrates. Medicina. 2025: 61: 118. https://doi.org/10.3390/medicina61010118.

[9] Zhou S, Linder KA, Kauffman CA, Richards BJ, Kleiboeker S, Miceli MH. Diagnostic Performance of Bronchoalveolar Lavage (1,3)-β-d-Glucan Assay for *Pneumocystis jirovecii* Pneumonia. Journal of Fungi (Basel, Switzerland). 2020; 6: 200. https://doi.org/10.3390/jof6040200.

[10] Torres A, Niederman MS, Chastre J, Ewig S, Fernandez-Vandellos P, Hanberger H, *et al*. International ERS/ESICM/ESCMID/ALAT guidelines for the management of hospital-acquired pneumonia and ventilator-associated pneumonia: Guidelines for the management of hospital-acquired pneumonia (HAP)/ventilator-associated pneumonia (VAP) of the European Respiratory Society (ERS), European Society of Intensive Care Medicine (ESICM), European Society of Clinical Microbiology and Infectious Diseases (ESCMID) and Asociación Latinoamericana del Tórax (ALAT). The European Respiratory Journal. 2017; 50: 1700582. https://doi.org/10.1183/13993003.00582-2017.

[11] Zhong CH, Su ZQ, Luo WZ, Rao WY, Feng JX, Tang CL, *et al*. Hierarchical clock-scale hand-drawn mapping as a simple method for bronchoscopic navigation in peripheral pulmonary nodule. Respiratory Research. 2022; 23: 245. https://doi.org/10.1186/s12931-022-02160-0.

[12] Xu C, Wang Y, Li L, Yuan Q, Wang Y, Hu H, *et al*. Diagnostic Value of Virtual Bronchoscopic Navigation Combined With Endobronchial Ultrasound Guided Transbronchial Lung Biopsy for Peripheral Pulmonary Lesions. Technology in Can-

cer Research & Treatment. 2021; 20: 1533033821989992. https://doi.org/10.1177/1533033821989992.

[13] Wang S, Yang J, Luo S, Geng J, Ren Y, Zhao L, *et al*. The accuracy of electromagnetic navigation bronchoscopy compared to fluoroscopy in navigation of transbronchial lung cryobiopsy in patients with interstitial lung disease. BMC Pulmonary Medicine. 2024; 24: 108. https://doi.org/10.1186/s12890-024-02925-x.

[14] Liu M, Zhang H, Li L, Mao J, Li R, Yin J, *et al*. The etiological diagnostic value of metagenomic next-generation sequencing in suspected community-acquired pneumonia. BMC Infectious Diseases. 2024; 24: 626. https://doi.org/10.1186/s12879-024-09507-6.

[15] Zhao Y, Zhang W, Zhang X. Application of metagenomic next-generation sequencing in the diagnosis of infectious diseases. Frontiers in Cellular and Infection Microbiology. 2024; 14: 1458316. https://doi.org/10.3389/fcimb.2024.1458316.

[16] Nan X, Yu J, Liang Y, Lou P, Pan G. Application of Different Sampling Methods Combined with Metagenomic Next-Generation Sequencing to Detect Pathogens in Children with Severe Pneumonia on Mechanical Ventilation. Infection and Drug Resistance. 2023; 16: 4545–4553. https://doi.org/10.2147/IDR.S418339.

[17] Shi Y, Peng JM, Qin HY, Du B. Metagenomic next-generation sequencing: A promising tool for diagnosis and treatment of suspected pneumonia in rheumatic patients with acute respiratory failure: Retrospective cohort study. Frontiers in Cellular and Infection Microbiology. 2022; 12: 941930. https://doi.org/10.3389/fcimb.2022.941930.

[18] Qu JM, Cao B. Guidelines for the diagnosis and treatment of adult community acquired pneumonia in China (2016 Edition). Zhonghua Jie he he Hu Xi Za Zhi = Zhonghua Jiehe he Huxi Zazhi = Chinese Journal of Tuberculosis and Respiratory Diseases. 2016; 39: 241–242. https://doi.org/10.3760/cma.j.issn.1001-0939.2016.04.001.

[19] de Palma TH, Powers C, McPartland MJ, Mark Welch J, Ramsey M. Essential genes for *Haemophilus parainfluenzae* survival and biofilm growth. MSystems. 2024; 9: e0067424. https://doi.org/10.1128/msystems.00674-24.

[20] Davis NM, Proctor DM, Holmes SP, Relman DA, Callahan BJ. Simple statistical identification and removal of contaminant sequences in marker-gene and metagenomics data. Microbiome. 2018; 6: 226. https://doi.org/10.1186/s40168-018-0605-2.

[21] Deng J, Chen X, Bu Y, Zhang J, Han J. Exploring the appropriate situation of performing CSF mNGS in patients with proposed intracranial infections. BMC Neurology. 2024; 24: 429. https://doi.org/10.1186/s12883-024-03925-4.

[22] Tsai YM, Kuo YS, Lin KH, Chen YY, Huang TW. Diagnostic Performance of Electromagnetic Navigation versus Virtual Navigation Bronchoscopy-Guided Biopsy for Pulmonary Lesions in a Single Institution: Potential Role of Artificial Intelligence for Navigation Planning. Diagnostics (Basel, Switzerland). 2023; 13: 1124. https://doi.org/10.3390/diagnostics13061124.

[23] Yuan M, Hu Y, Wang L, Yin W, Xiao Y. Diagnostic outcomes of radial endobronchial ultrasound bronchoscopy guided by manual navigation in the evaluation of peripheral pulmonary lesions: An observational study. The Clinical Respiratory Journal. 2024; 18: e13768. https://doi.org/10.1111/crj.13768.

[24] Katsis J, Roller L, Aboudara M, Pannu J, Chen H, Johnson J, *et al*. Diagnostic Yield of Digital Tomosynthesis-assisted Navigational Bronchoscopy for Indeterminate Lung Nodules. Journal of Bronchology & Interventional Pulmonology. 2021; 28: 255–261. https://doi.org/10.1097/LBR.0000000000000766.

[25] Zar HJ, Andronikou S, Nicol MP. Advances in the diagnosis of pneumonia in children. BMJ (Clinical Research Ed.). 2017; 358: j2739. https://doi.org/10.1136/bmj.j2739.

[26] Zhang Y, Zhou H, Jiang Q, Wang Q, Li S, Huang Y. Bronchoscope-related Pseudomonas aeruginosa pseudo-outbreak attributed to contaminated rinse water. American Journal of Infection Control. 2020; 48: 26–32. https://doi.org/10.1016/j.ajic.2019.06.013.

[27] Grønseth R, Drengenes C, Wiker HG, Tangedal S, Xue Y, Husebø GR, *et al*. Protected sampling is preferable in bronchoscopic studies of the airway microbiome. ERJ Open Research. 2017; 3: 00019–2017. https://doi.org/10.1183/23120541.00019-2017.

[28] Chioma OS, Hesse LE, Chapman A, Drake WP. Role of the Microbiome in Interstitial Lung Diseases. Frontiers in Medicine. 2021; 8: 595522. https://doi.org/10.3389/fmed.2021.595522.

[29] Kanaoka K, Minami S, Ihara S, Komuta K. High neutrophils and low lymphocytes percentages in bronchoalveolar lavage fluid are prognostic factors of higher in-hospital mortality in diffuse alveolar hemorrhage. BMC Pulmonary Medicine. 2021; 21: 288. https://doi.org/10.1186/s12890-021-01660-x.

[30] Wang C, Hu ZW, Li ZY, Zhao MH, Little MA, Chen M. Advantages of metagenomic next-generation sequencing in the management of ANCA-associated vasculitis patients with suspected pulmonary infection as a rule-out tool. BMC Pulmonary Medicine. 2024; 24: 478. https://doi.org/10.1186/s12890-024-03301-5.